A. GÓRAL*, L. LITYŃSKA-DOBRZYŃSKA*, W. ŻÓRAWSKI**, K. BERENT*, J. WOJEWODA-BUDKA*

MICROSTRUCTURE OF Al₂O₃-13TiO₂ COATINGS DEPOSITED FROM NANOPARTICLES BY PLASMA SPRAYING

MIKROSTRUKTURA POWŁOK Al₂O₃-13TiO₂ NATRYSKANYCH PLAZMOWO Z NANOCZĄSTEK

The aim of the study was to characterize nanostructured Al_2O_3-13TiO_2 coatings deposited by plasma spraying on a grit blasted steel substrate. The Al_2O_3-13TiO_2 coatings were characterized using scanning and transmission electron microscopy and X-ray diffraction techniques. Obtained coatings possessed a unique microstructure consisting of fully melted regions with the microstructure similar to a typical plasma sprayed lamellar morphology as the conventional coatings and areas comprising unmelted or partially melted nanosized particles. The analysis showed that most of the α-Al_2O_3 phase from the nanostructured powders transformed into γ-Al_2O_3 phase after plasma spraying process. Moreover, the presence of amorphous phase was also observed.

Keywords: Al_2O_3-13TiO_2 coating, microstructure, plasma spraying process

W pracy przedstawiono charakterystykę nanostrukturalnych powłok Al_2O_3-13TiO_2 natryskiwanych plazmowo na podłożu stalowym. Powłoki scharakteryzowano za pomocą skaningowej i transmisyjnej mikroskopii elektronowej oraz technik dyfrakcji rentgenowskiej. Mikrostruktura uzyskanych powłok składała się z obszarów powstałych z całkowicie stopionych proszków, podobnych do mikrostruktury powłok wytworzonych z proszków o rozmiarach konwencjonalnych, jak również z obszarów zawierających niestopione lub częściowo stopione nanocząstki. Wykazano, że większość fazy α-Al_2O_3 występującej w materiale proszkowym uległa przemianie w fazę γ-Al_2O_3 w trakcie procesu natryskiwania plazmowego. Zidentyfikowano również obecność fazy amorficznej.

1. Introduction

In recent years, plasma-sprayed nanostructured ceramic coatings have attracted wide interest because of their better properties compared to the conventional counterparts. In particular, coatings made of Al_2O_3 containing 13% TiO_2 are commonly used to improve the wear, corrosion and erosion resistance of steels [1,2]. Although the coatings produced by thermal spraying possess numerous defects, such as pores and microcracks, the process efficiency is much higher and the costs are considerably lower, compared to those obtained by other processes (e.g. atomic layer deposition, cyclic chemical vapour deposition) [3]. In this process, a coating material (usually in a form of a powder) is injected into a plasma stream where it is heated and accelerated toward the substrate. After impacting the surface the ceramic rapidly cools and forms a coating. The possibility of producing nanostructured coatings with superior properties (e.g. wear resistance) compared to the conventional thermal spray coatings currently available opens a wide range of research opportunities for different materials. In thermal spray processes, materials in wire or powder form are fed into a flame, arc or plasma spray gun, where they are fully or partially melted and accelerated in a gas stream toward a substrate to be coated. As compared to traditional plasma spray process, plasma spraying of nanostructured materials introduces a number of complications. Nanostructured materials cannot be fed directly into the spray guns. They are deposited in the form of suspensions, or powders which grains are agglomerated nanocrystals [4-6]. Alumina with different content of titania is widely used in industry to improve the wear resistance of machine parts. The Al_2O_3-13TiO_2 thermally sprayed coatings are well established as materials highly resistant to wear in a wide variety of applications [2,7,8]. Therefore nanostructured Al_2O_3-13TiO_2 coatings are of particular scientific interest because of their physical and mechanical properties, which are superior to those of conventional materials.

The aim of the present study was to determine the microstructure of nanostructured composite Al_2O_3-13TiO_2 coatings plasma sprayed on a steel substrate combined with phase analysis, morphology, residual stress and hardness measurements.

2. Experimental

The plasma spray process was carried out with the Plancer PN-120 gun equipped with the Thermal Miller 1264 powder feeder. The raw material powders consisted mainly of

*   INSTITUTE OF METALLURGY AND MATERIALS SCIENCE, POLISH ACADEMY OF SCIENCES, KRAKÓW, POLAND
** FACULTY OF MECHATRONICS AND MACHINE BUILDING, KIELCE UNIVERSITY OF TECHNOLOGY, KIELCE, POLAND

α-Al$_2$O$_3$ and TiO$_2$ (Al$_2$O$_3$: TiO$_2$ wt ratio = 87:13), ZrO$_2$ ($\sim$8 wt %) and CeO$_2$ ($\sim$5 wt%) powders. Such additives are mainly added to powder in order to lower the sintering temperature and accelerate the densification process [9]. The plasma generated for plasma spraying incorporated a mixture of argon (primary plasma gas) and hydrogen (secondary plasma gas), the latter constituting 7% of the mixture volume. The coatings were deposited on flat samples in low-carbon steel with dimensions of 30 x 30 x 3 mm. Before spraying, the substrate had to be degreased and grit blasted with electrocorundum EB-16 at a pressure of 0.5 MPa. The parameters of plasma spraying were as follows: current of 550 A, voltage of 55 V, plasma gas pressure of 0.7 MPa, spray distance of 100 mm, powder feeding rate of 90 g/min.

The morphology of both the top surface and cross section of obtained nanostructured Al$_2$O$_3$-13TiO$_2$ coatings were characterized using scanning electron microscopy (SEM) – FEI QUANTA 3D FEG, however a detailed analysis of Al$_2$O$_3$-13TiO$_2$ powder and cross section of coating were performed with transmission electron microscopy (TEM) – FEI TECNAI G^2. The thin foils were prepared by Focused Ion Beam (FIB) technique using FEI QUANTA 3D Dual Beam from the cross section of the coating. The X-ray diffraction techniques (Bruker D8 diffractometer with CoKα filtered radiation) were used for phase analysis and measurement of residual stresses. The hardness of the coatings was measured by Vicker's universal hardness tester Zwick/Roell ZHU250 with a load of 0.5 kG.

3. Microstructure of Al$_2$O$_3$-13TiO$_2$ coatings

The feedstock used for plasma spraying of nanostructured Al$_2$O$_3$-13TiO$_2$ coatings was composed of spherical agglomerates with sizes in the range 10-50 μm derived from nanoparticles. Fig. 1 presents SEM secondary electrons (SE) micrograph of feedstock of spherical morphology (Fig. 1a) and TEM bright field (BF) micrograph of α-Al$_2$O$_3$, TiO$_2$, ZrO$_2$, CeO$_2$ nanoparticles (Fig. 1b) derived from disintegrated agglomerate. The spherical powders possess excellent flow ability owing to their roundness and smoothness.
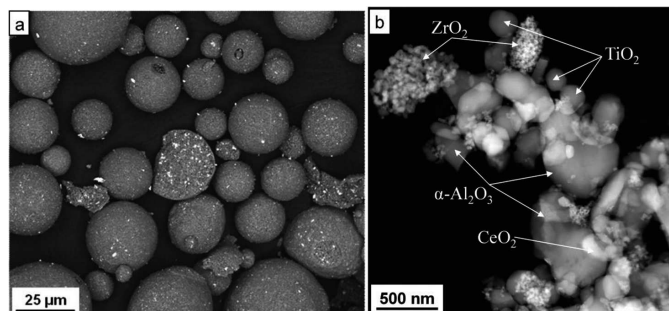

Fig. 1. Microstructure of nanostructured Al$_2$O$_3$-13TiO$_2$ thermal spray powders a) SEM SE (secondary electrons) micrograph of agglomerated nanoparticles (feedstock of spherical morphology); b) TEM BF (bright field) micrograph of Al$_2$O$_3$, TiO$_2$, ZrO$_2$, CeO$_2$ nanoparticles

The XRD patterns of nanostructured powders and obtained coatings are shown in Fig. 2. The average coating thickness was about 850 μm.

The analysis showed that most of α-Al$_2$O$_3$ (rhombohedral, a = 4.759 Å, c = 12.993 Å) in the nanostructured powders transformed into γ-Al$_2$O$_3$ (cubic, a = 7.938 Å) after plasma spraying process. It is well establish that because of a higher cooling rate γ-Al$_2$O$_3$ commonly nucleates in preference to α-Al$_2$O$_3$ during rapid solidification of the liquid droplets [8]. The γ-Al$_2$O$_3$ phase forms more easily from the melt than α-Al$_2$O$_3$ at a high cooling rate, because of the low interfacial energy between crystal and liquid [10]. The XRD phase analysis revealed that the volume fraction of γ-Al$_2$O$_3$ was about 60%. The crystallite sizes, estimated by peak broadening analysis, were 23 nm and 77 nm for γ-Al$_2$O$_3$ and α-Al$_2$O$_3$ phases, respectively. During plasma spraying, nanostructured powders behaved differently in terms of thermal response due to the distribution of the powder size and the temperature in plasma jet [11]. The α-Al$_2$O$_3$ phase originated from the presence of unmelted or partially melted alumina. XRD patterns suggest that α-Al$_2$O$_3$ particles were not completely transferred to soften γ-Al$_2$O$_3$ after the flame-spray process. This result is important from tribological behaviour point of view since hardness plays an important role with regards to wear resistance [11-13].
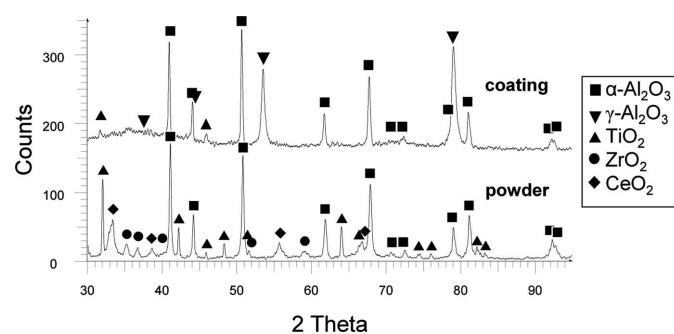

Fig. 2. XRD patterns of Al$_2$O$_3$-13TiO$_2$ powder and coating after plasma spraying process

Figure 3 presents scanning electron microscopy image taken at the backscattered electrons mode of the top surface (Fig. 3a) and cross section (Figs. 3b, c) of the Al$_2$O$_3$-13TiO$_2$ coatings.

The coatings possessed a unique microstructure consisting of fully melted regions with the microstructure similar to a typical plasma sprayed lamellar morphology as conventional coatings and regions comprising unmelted or partially melted nanosized particles. It was observed that most powders were fully or partially melted during plasma spraying. The fraction of unmelted or partially melted regions in the nanostructured coatings is mainly connected with the increase in the plasma spray power as more powder is melted. In the SEM images γ-Al$_2$O$_3$ phase is recognizable by light grey contrast, partially melted particles by grey colour with a spherical morphology and pores appearing as holes. The fully melted (A) regions mainly consisted of nanocrystalline γ-Al$_2$O$_3$, while the partially melted (B) areas were composed of α-Al$_2$O$_3$ grains embedded into γ-Al$_2$O$_3$ matrix (Fig. 3c). An exemplary unmelted particle is marked as C in Fig. 3c.

Bright field transmission electron microscopy image of the cross section of Al$_2$O$_3$-13TiO$_2$ coating and the maps of distribution of particular elements (Al, O, Ti, Zr, Ce) are presented in Fig. 4.

It could be seen that fully melted region (the upper-right part in the Fig. 4a) contains mainly aluminium and oxygen without distinguishable changes in the chemical composition. This area was formed from fully melted oxide components. In contrast, the distribution of the elements are not homogenous in the vicinity of unmelted particles. Concentration of Ti, Zr, Ce increases within the spaces between Al_2O_3 particles, what is clearly visible in Figs. 4d-f.
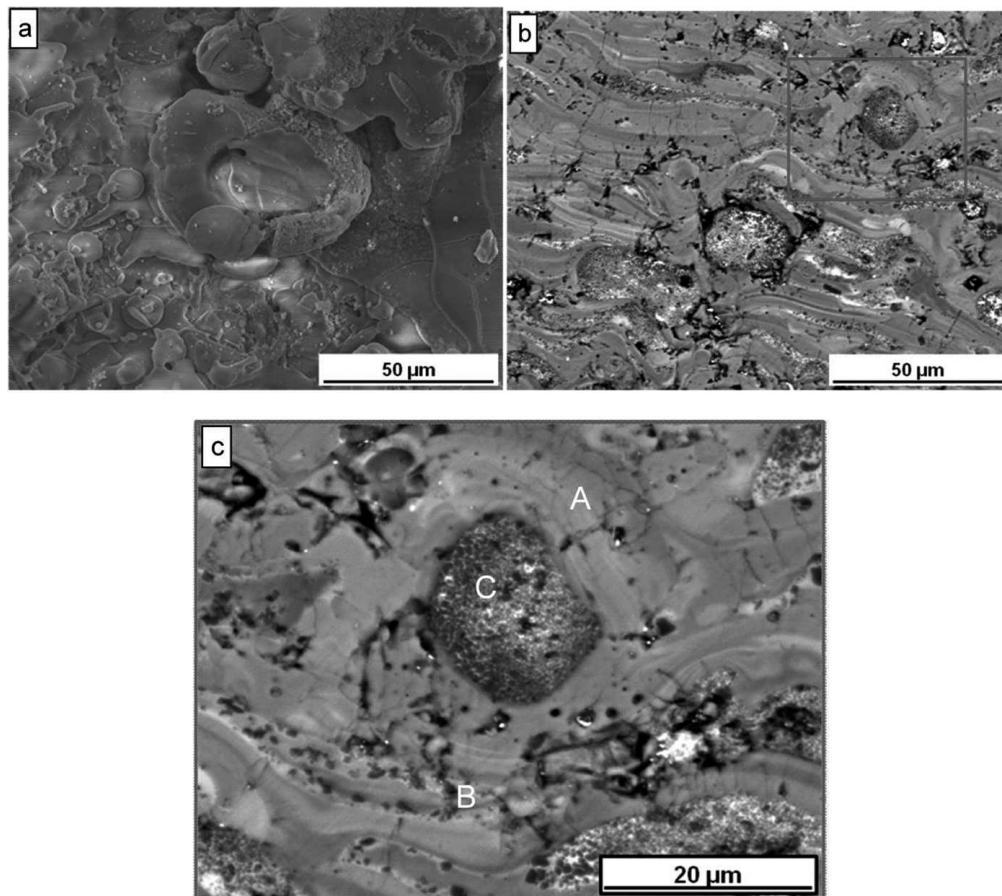

Fig. 3. SEM BSE microstructure of obtained nanostructured Al_2O_3-13TiO_2 coating: a) top surface, b) cross section, c) high magnification of selected area of cross section (A – fully melted region, B – partially melted region, C – unmelted region)
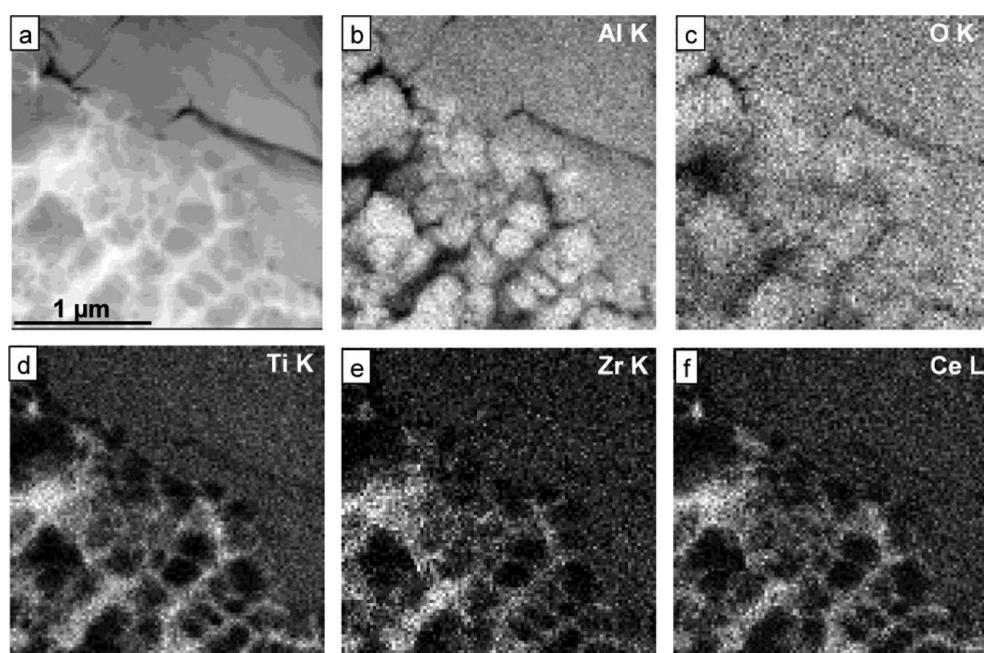

Fig. 4. Bright field TEM image of exemplary cross section and maps of distribution of Al, O, Ti, Zr, Ce elements in presented area
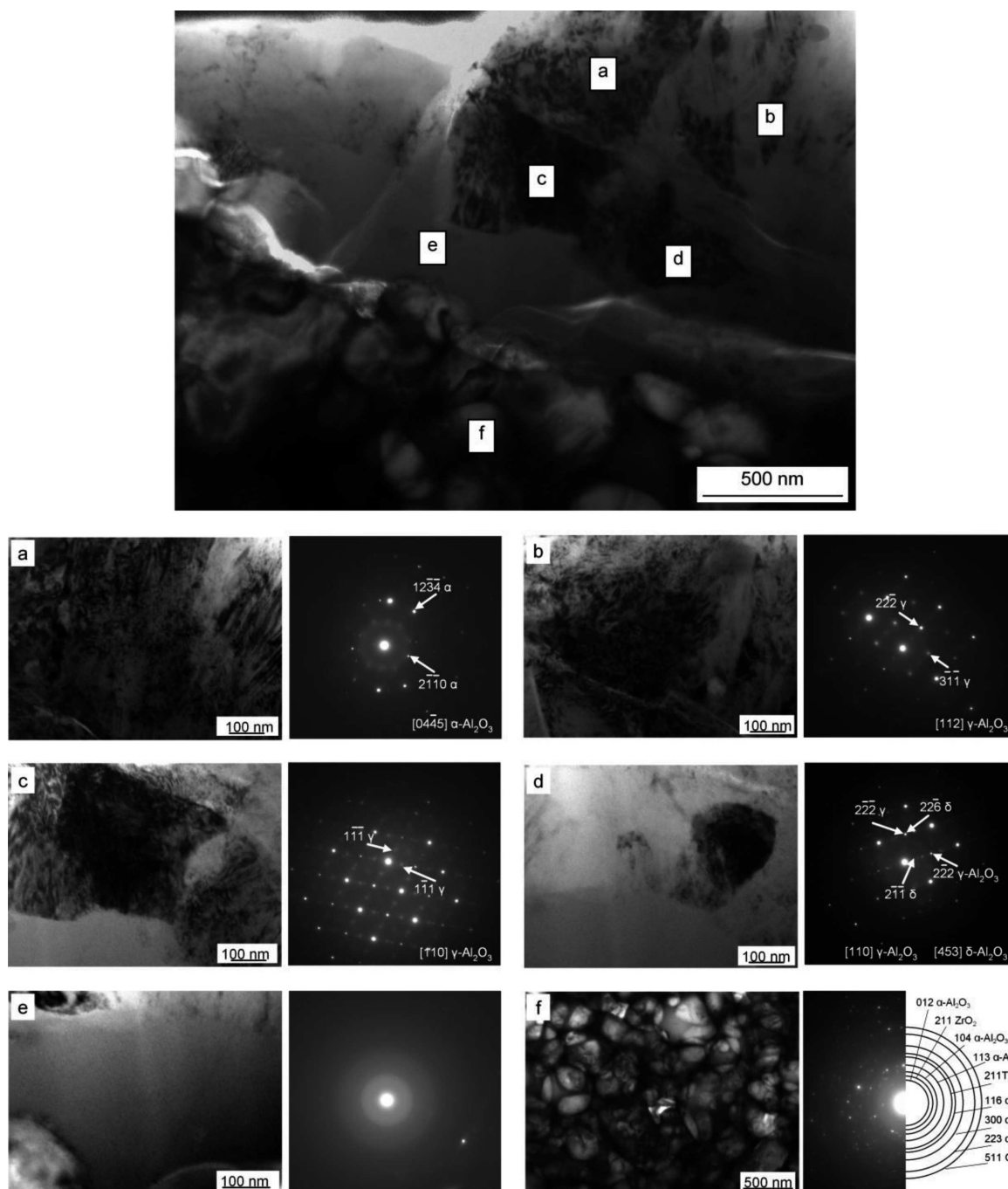
www.czasopisma.pan.pl PAN www.journals.pan.pl

Fig. 5. Bright field TEM image of Al_2O_3-13TiO_2 coating cross section representing the fully melted region in contact with unmelted particles, a-f) higher magnification of marked parts and corresponding SADPs

Figure 5 shows TEM bright-field (BF) images of the rounded features (unmelted/partially melted particles) in contact with the fully melted region (similar to that presented in Fig. 4a) and enlarged images of marked parts with corresponding selected area diffraction patterns (SADPs) obtained from these areas. The detailed TEM study revealed that region of homogeneous chemical composition presented in Fig. 4 contains mixture of the nanocrystalline grains with different crystal structure: α-Al_2O_3 phase (Fig. 5a) and for the most part γ-Al_2O_3 (Figs. 5b-d). Based on the analysis of SADPs differently oriented γ-Al_2O_3 grains were identified. TEM observations revealed also a presence of tetragonal δ-Al_2O_3 phase with lattice constants: $a_\delta = b_\delta = 7.961$ Å ($a_\delta = b_\delta \approx a_\gamma$) and $c_\delta = 23.43$ Å ($c_\delta \approx 3a_\gamma$), although this phase has not been detected with XRD technique (see Fig. 2). This phase coexisted with the γ-Al_2O_3 phase (see Fig. 5d). The δ-Al_2O_3 phase has been described in [14] as a superlattice of a spinel structure. Between nanocrystalline phases and unmelted/partially melted area the amorphous phase was identified (Fig. 5e). It was formed possibly due to fast cooling rates encountered in this process. The SADP of partially melted particles showed that in this area all initial phase components of powder: α-Al_2O_3 (mainly), TiO_2, ZrO_2 and CeO_2 coexisted (Fig. 5f). The indexing of ring diffraction pattern shown in Fig. 5f was performed using ProcessDiffraction program [15].

4. Residual stresses and hardness of Al$_2$O$_3$-13TiO$_2$ coatings

Table 1 presents values of residual stresses and hardness of Al$_2$O$_3$-13TiO$_2$ coatings. Residual stresses of examined coatings were measured for (440) plane ($2\theta \approx 79.58°$) using X-ray diffraction technique. Values of the stresses were calculated considering the diffraction elastic constants [16] by the Reuss model using a computer program Stress [17]. Evaluated residual stresses are mean values for the volume defined by the cross section of X-ray beam and by the penetration depth of the used radiation. The stresses have been calculated by $\sin^2 \psi$ procedure. The estimated residual stresses in the coatings were of tensile character and their values were about 230 MPa.

TABLE 1

Residual stress and hardness of Al$_2$O$_3$-13TiO$_2$ coating

Coating	Residual stress [MPa]	Hardness HV0.5
Al$_2$O$_3$-13TiO$_2$	229 ± 36	931 ± 117

The final hardness value determined at level 931 HV0.5 is an average of 7 measurements performed at different locations on the coating cross section. They are in agreement with the work by Zhang et al. [11].

5. Conclusions

The feedstock used for plasma spraying of nanostructured materials was composed agglomerates formed from nanoparticles because nanopowders cannot be fed directly into the spray guns. The obtained Al$_2$O$_3$-13TiO$_2$ coatings possessed a unique microstructure consisting of fully melted regions (typical plasma sprayed lamellar-like structures as the conventional coatings) and regions comprising unmelted or partially melted nanosized particles.

Most of α-Al$_2$O$_3$ (rhombohedral) phase in the nanostructured powders transformed into γ-Al$_2$O$_3$ (cubic) during plasma spraying process. TEM investigations revealed also the presence of δ-Al$_2$O$_3$ (tetragonal) phase in the microstructure of the coating. Moreover, the amorphous phase existing between grains of nanocrystalline phases and unmelted/partially melted particles was observed.

The residual stresses estimated in the coatings were of tensile character and their values were at the level of 230 MPa, whereas hardness of the coatings was about 930 HV0.5.

REFERENCES

[1] R.B. H e i m a n n, Key Eng. Mater. **122-124**, 399 (1996).
[2] J. Z h a n g, J. H e, Y. D o n g, X. L i, D. Y a n, J. Mater. Process. Tech. **197**, 31 (2008).
[3] P.C. R o w l e t t e, C.A. W o l d e n, Thin Solid Films **518**, 3337 (2010).
[4] P. F a u c h a i s, G. M o n t a v o n, G. B e r t r a n d, J. Therm. Spray Techn. **19**, 56 (2010).
[5] R.S. L i m a, K.A. K h o r, H. L i, P. C h e a n g, B.R. M a r p l e, Mater. Sci. Eng. A, **396**, 181 (2005).
[6] G. B o l e l l i, V. C a n n i l l o, R. G a d o w, A. K i l l i n g e r, L. L u s v a r g h i, J. R a u c h, M. R o m a g - n o l i, Surf. Coat. Tech. **204**, 1163 (2010).
[7] W. T i a n, Y. W a n g, Y. Y a n g, C. L i, Surf. Coat. Tech. **204**, 642 (2009).
[8] D. W a n g, Z. T i a n, L. S h e n, Z. L i u, Y. H u a n g, Surf. Coat. Tech. **203**, 1298 (2009).
[9] Y. Y a n g, Y. W a n g, Z. W a n g, G. L i u, W. T i a n, Mater. Sci. Eng. A **490**, 457 (2008).
[10] X. L i n, Y. Z e n g, X. Z h o u, C. D i n g, Mater. Sci. Eng. A **357**, 228 (2003).
[11] J. Z h a n g, J. H e, Y. D o n g, X. L i, D. Y a n, Rare Metals **26**, 391 (2007).
[12] I.M. K u s o g l u, E. C e l i k, H. C e t i n e l, I. O z d e m i r, O. D e m i r k u r t, K. O n e l, Surf. Coat. Tech. **200**, 1173 (2005).
[13] E. S a n c h e z, E. B a n n i e r, V. C a n t a v e l l a, M.D. S a l v a d o r, E. K l y a t s k i n a, J. M o r g i e l, J. G r z o n - k a, A.R. B o c c a c c i n i, J. Therm. Spray Techn. **17**, 329 (2008).
[14] I. L e v i n, D. B r a n d o n, J. Am. Ceram. Soc. **81**, 1995 (1998).
[15] J.L. L a b a r, Ultramicroscopy **103**, 237 (2005).
[16] G. S i m m o n s, H. W a n g, Single Crystal Elastic Constant and Calculated Aggregate Properties. The M.I.T Press 1971.
[17] A. B a c z m a ń s k i, Program Stressfit, AGH, Krakow 2004.